

Review

# Multilevel Diffractive Lenses: Recent Advances and Applications

Chenyu Shi <sup>1</sup>, Weipeng Zhao <sup>1</sup>, Sai Chen <sup>1,\*</sup> and Wenli Li <sup>2,3,\*</sup>

<sup>1</sup> School of Electronic Information Engineering, Beihang University, Beijing 100191, China; chenyushi@buaa.edu.cn (C.S.); zy2202507@buaa.edu.cn (W.Z.)

<sup>2</sup> Ningbo Institute of Northwestern Polytechnical University, Ningbo 315103, China

<sup>3</sup> College of Mechanical Engineering, Northwestern Polytechnical University, Xi'an 710072, China

\* Correspondence: saichen@buaa.edu.cn (S.C.); wenlili\_mems@nwpu.edu.cn (W.L.)

**Abstract:** Multilevel diffractive lenses (MDLs) has undergone considerable advancements, marked by their exceptional efficiency and diverse focusing capabilities, resulting in their widespread use in optical systems. In recent times, MDLs have consistently been juxtaposed with metalenses, which have experienced swift progress over the last decade. Concurrently, MDLs have continued to evolve, propelled by their distinct advantages, such as cost-effective production and adaptability for mass manufacturing. This article explores the evolution and foundational concepts of MDLs, highlighting the advantages of their circular symmetry in enhancing simulation and optimization efficiency. Furthermore, we present several innovative fabrication methods for MDLs that capitalize on the latest advancements in 3D printing technology. We also show the practical applications and potential future developments of MDLs.

**Keywords:** multilevel diffractive lens; cylindrical FDTD; 3D printing



**Citation:** Shi, C.; Zhao, W.; Chen, S.; Li, W. Multilevel Diffractive Lenses: Recent Advances and Applications. *Symmetry* **2024**, *16*, 1377. <https://doi.org/10.3390/sym16101377>

Academic Editor: Sergei Odintsov

Received: 31 August 2024

Revised: 29 September 2024

Accepted: 14 October 2024

Published: 16 October 2024



**Copyright:** © 2024 by the authors. Licensee MDPI, Basel, Switzerland. This article is an open access article distributed under the terms and conditions of the Creative Commons Attribution (CC BY) license (<https://creativecommons.org/licenses/by/4.0/>).

## 1. Introduction

Optical lenses have been crucial components in various fields, such as microscopy and laser technology, where they act as the central pieces of optical systems. In classical wave optics, the manipulation of light propagation is mainly achieved through the phenomena of reflection, refraction, and diffraction. The governing principles of these processes are the law of reflection, Snell's law, and the grating equation, respectively [1]. Meanwhile, traditional optical systems rely heavily on large optical components such as convex lenses and parabolic mirrors, which operate based on the principles of refraction and reflection, respectively. However, traditional lenses that operate on the principle of refraction are terribly affected by the Rayleigh diffraction limit. Furthermore, the reliance on convex lenses hinders the progress of optical systems towards achieving greater compactness and integration.

To relieve the effect of this limitation, there is a growing emphasis on the importance of optical diffraction devices, which are compact and easily integrated into systems [2–4]. These devices have the potential to revolutionize the field by enabling the creation of more compact, efficient, and highly integrated optical systems. Due to their compactness and ease of integration, diffractive devices are increasingly playing key roles in the advancement of optical technology, for example the planar lenses.

Over the past few decades, significant progress has been made in developing planar lenses [5], known for their lightweight, thin profiles, and high efficiency, as well as their capacity to handle the Rayleigh diffraction limit. [6].

A range of planar lenses has been brought to fruition through the concerted efforts of numerous researchers, as depicted in the Figure 1, which exemplifies the relationships between different planar lenses. Among these, Fresnel zone plates (FZPs) stand out as an exemplary type of Fresnel lenses that embodies feature of compact sizes [7–10]. However,

the fabrication capability may affect the diffraction efficiency of FZPs [11]. Consequently, a more efficient type of planar lenses, specifically the multilevel diffractive lenses (MDLs), is increasingly capturing the interest of researchers, showed in Figure 2.

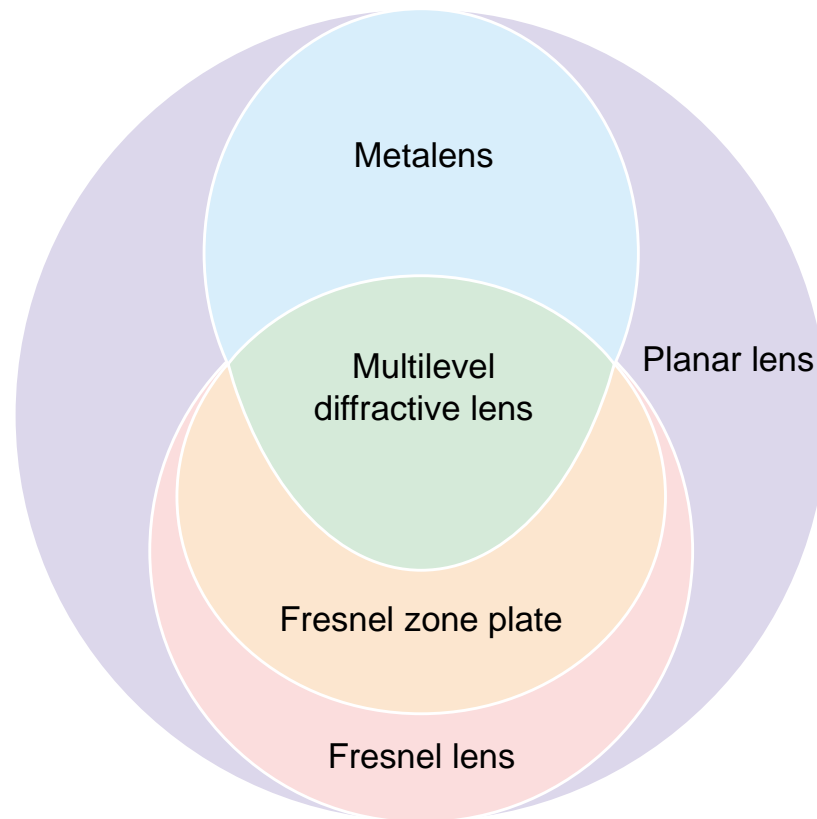


**Figure 1.** The category of planar lenses comprises Fresnel lenses, Fresnel zone plates, and the quickly developing field of metalenses, which have made significant progress in recent years. Researchers posit that multilevel diffractive lenses (MDLs), which have evolved from the principles of Fresnel lenses, share many common functionalities with metalenses and are sometimes considered a novel class of metalenses.

MDLs provide a substantially greater degree of freedom compared to FZPs [12]. As a result, MDLs can achieve a relatively high efficiency and have potential applications across a variety of fields, including imaging [13,14], optical communications, holography, and virtual reality [15]. There has also been examples of MDLs working range from keV X-rays [16], ultraviolet [17], visible light to infrared [18], terahertz frequencies [19]. The benefits of MDLs include their compact size, lightweight construction, and compatibility with the integration of other optical components. These attributes render them highly suitable for use in compact optical systems, particularly those found in mobile devices and micro-optical systems.

In the last decade, the emergence of metasurfaces which alter the amplitude, phase, and polarization of light through the use of structures smaller than the wavelength of light has paved the way for researchers to delve into the design and manufacturing of metalenses across an extensive spectrum of wavelengths, extending from the visible light spectrum to infrared and terahertz frequencies [20–23]. However, it's crucial to recognize that the current research on metalenses is mainly concentrated on materials with high refractive indices or metals, which results in complex manufacturing processes. Consequently, the cost of producing metalenses remains excessively high, which hinders their mass production and large-scale manufacturing capabilities.

Currently, there is an increasing perspective that MDLs can be considered as metalenses when their structures are reduced to the sub-wavelength scale [24,25]. This under-

scores the vast potential of MDLs across various contemporary optics disciplines, offering researchers substantial incentive to continue advancing and make further progress in this domain.

However, the production of MDLs can be quite demanding due to the exacting requirements of their multilevel structure. Fabrication methods like electron-beam lithography (EBL) and direct laser ablation (DLA) are frequently employed for creating MDLs, but these necessitate complex manufacturing processes. The complexity of fabrication has historically posed a challenge to the development of MDLs, slowing progress in the field since the previous century.

In this article, we will begin by examining the principles of MDLs, including the design and simulation processes. This involves innovative inverse design methods and electromagnetic simulation techniques that relying on the capabilities of modern computing. These advanced tools have significantly enhanced our ability to refine and evaluate the performance of MDLs. Next, we will focus on the prevalent fabrication techniques employed for MDLs, highlighting how emerging additive manufacturing technologies offer advantages over conventional lithography methods. We will delve into the progress that has been made in this area, as well as explore the emerging applications and the potential future developments in the field of MDLs.

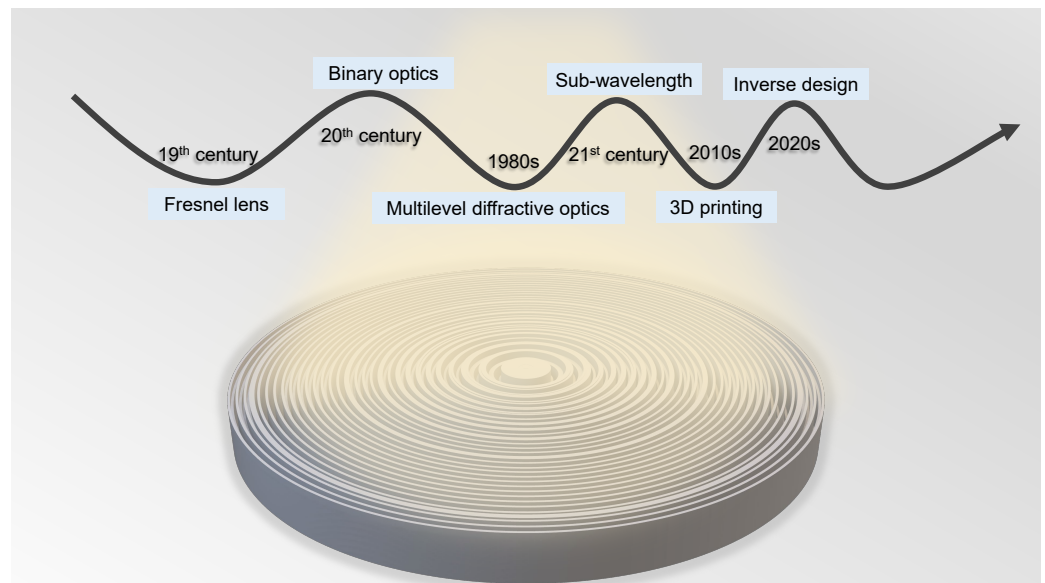


**Figure 2.** The research in Fresnel lens concept by Augustin-Jean Fresnel in the 19th century represented a significant early development in the field of diffractive optics. As laser technology emerged and there was a demand for more efficient optical components, binary diffractive optics, such as FZPs, were invented in the 20th century. The late 20th century saw the evolution of multilevel diffractive optics to enhance efficiency and expand functionality. In the 21st century, advancements in MDLs included the creation of sub-wavelength structures, the utilization of 3D printing technology, and the adoption of inverse design methods.

## 2. Principles

Multilevel diffractive lenses (MDLs) and metalenses are promising optical technologies that surpass traditional lenses by utilizing multiple discrete phase levels to manipulate light wavefronts. This results in improved focusing performance, such as high numerical aperture (NA) and the correction of optical aberrations. Typically, these lenses are made from dielectric materials such as silicon and are designed using optimization algorithms and inverse design methods. In the case of metalenses, nanostructures are meticulously patterned on a sub-wavelength scale to produce the desired optical performance. MDLs also require a similar patterning to achieve specific phase profiles. Fortunately, the circular symmetry characteristic of MDLs allows for electromagnetic simulations to be conducted

in cylindrical coordinates, significantly reducing the computation time required for finite-difference time-domain (FDTD) methods, which are essential for inverse design processes.

### 2.1. Optical Path Difference

Figure 3a depicts the illustration of a MDL, highlighting the ring structures characterized by their width  $w$ , heights  $h$  and radial distances  $r$ . In the case of a chromatic MDL designed to function at a specific wavelength  $\lambda_0$  and with a given focal length  $f$ , the phase profile  $\varphi_{MDL}$  must conform to the equation Equation (1):

$$\varphi_{MDL}(r) = \frac{2\pi}{\lambda_0} \left( f - \sqrt{r^2 + f^2} \right) \quad (1)$$

where  $r$  represents the radial distance. This equation ensures that the MDL is capable of focusing light at the desired wavelength and focal point.

To attain the phase profile  $\varphi_{MDL}$  as described by the equation Equation (1), the individual rings of the MDL must introduce a phase change that corresponds to their radial position  $r$ . The optical path length through the dielectric material, which has a refractive index  $n$ , can be expressed as the product of the ring's height  $h_{MDL}(r) \cdot n$  and the refractive index  $n$ . Consequently, the difference in optical path length relative to that through free space is given by  $h_{MDL}(r) \cdot (n - 1)$ .

This optical path length difference translates to a phase difference  $\varphi_{MDL}$ , which is calculated by the formula Equation (2):

$$\varphi_{MDL}(r) = h_{MDL}(r) \cdot (n - 1) \frac{2\pi}{\lambda_0}. \quad (2)$$

Here,  $\lambda_0$  is the design wavelength. By equating this phase difference to the desired phase profile, we can derive the expression for the height of each ring, as shown in the equation for  $h_{MDL}(r)$  Equation (3). This relationship allows for the precise design of MDL ring heights to achieve the desired optical performance.

$$h_{MDL}(r) = \frac{\lambda_0}{2\pi(n - 1)} \varphi_{MDL}(r) \quad (3)$$

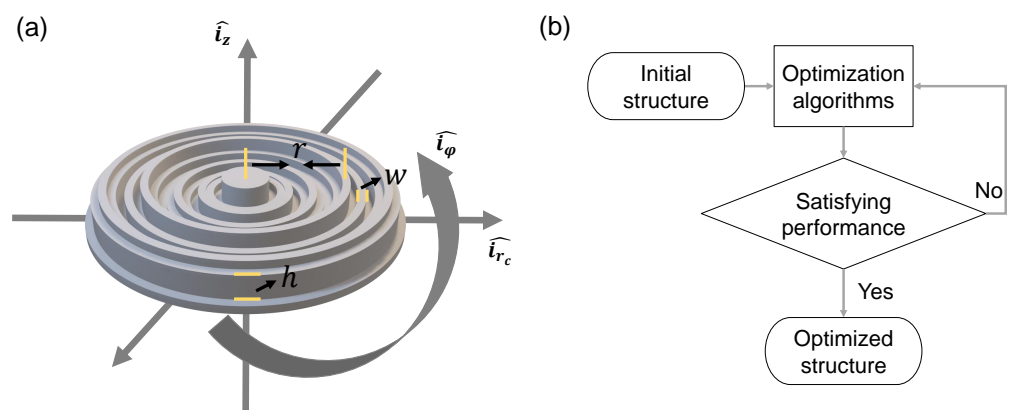


**Figure 3.** Illustration of MDL and inverse design methods. (a) The depiction of a MDL under cylindrical coordinates, the variable  $r$  denotes the radial distance from the lens's central axis,  $w$  signifies the width of each concentric ring structure, and  $h$  corresponds to the heights of the individual ring cylinders that comprise the MDL. (b) The inverse design methodology initiates with a preliminary configuration of widths  $w$  and heights  $h$  associated with each radial distance  $r$ . Following the application of optimization algorithms, this leads to the refinement of the structure, culminating in a design that meets the specified performance criteria.

## 2.2. Cylindrical FDTD

The efficacy of MDLs is often assessed through sophisticated simulation methods, with the FDTD approach being widely utilized. This technique entails the discretization of the electromagnetic field in both spatial dimensions and the time domain, enabling computational processing by computers. Such simulations are instrumental in confirming the design accuracy of a MDL and in guaranteeing that its performance aligns with predefined specifications.

However, the computational demands of these simulations can be substantial, frequently necessitating considerable processing time and computational resources. Particularly, FDTD analyses, which require the management of a vast array of mesh points, often demand considerable memory resources. This is due to the large volume of data that must be processed and stored during the simulation, especially when high-resolution modeling is required for precise predictions of the MDL's optical behavior.

Researchers have been exploring solutions to the computational challenges associated with simulating MDLs, for example a nonuniform FDTD for simulation of MDLs has been promoted [26], which can provide more efficient simulations for MDLs by varying the grid size across the computational domain. This technique allows for higher resolution in critical areas while using a coarser grid elsewhere, thus reducing the overall computational resources required.

Additionally, the circular symmetry inherent in MDLs can be strategically utilized to simplify FDTD simulations. By taking advantage of the symmetry in the cylindrical coordinate system, the complexity of the simulation can be significantly reduced, leading to faster computation times and less demand on memory resources [19,27]. This approach is particularly beneficial for MDLs, as it aligns with their natural symmetry, making the cylindrical FDTD method an ideal choice for their analysis.

Here, we offer a straightforward theoretical examination of the cylindrical FDTD's capacity to effectively simulate an MDL. Considering the Ampère's circuital law with Maxwell's addition, the differential equation could be:

$$\nabla \times \mathbf{H} = \frac{\partial \mathbf{D}}{\partial t} + \mathbf{J}, \quad (4)$$

in cylindrical coordinate showed in Figure 3a, the curl of magnetic field  $\mathbf{H}$  could be represented by:

$$\begin{aligned} \nabla \times \mathbf{H} &= \frac{1}{r_c} \begin{vmatrix} \mathbf{i}_{r_c} & r_c \mathbf{i}_\varphi & \mathbf{i}_z \\ \frac{\partial}{\partial r_c} & \frac{\partial}{\partial \varphi} & \frac{\partial}{\partial z} \\ H_{r_c} & r_c H_\varphi & H_z \end{vmatrix} \\ &= \frac{1}{r_c} \left[ \mathbf{i}_{r_c} \left( \frac{\partial H_z}{\partial \varphi} - \frac{\partial r_c H_\varphi}{\partial z} \right) + \mathbf{i}_\varphi r_c \left( \frac{\partial H_{r_c}}{\partial z} - \frac{\partial H_z}{\partial r_c} \right) + \mathbf{i}_z \left( \frac{\partial r_c H_\varphi}{\partial r_c} - \frac{\partial H_{r_c}}{\partial \varphi} \right) \right], \end{aligned} \quad (5)$$

and the partial derivative of electric field  $\mathbf{D}$  with current  $\mathbf{J}$  could be written as:

$$\begin{aligned} \frac{\partial \mathbf{D}}{\partial t} + \mathbf{J} &= \frac{\partial \varepsilon \mathbf{E}}{\partial t} + \sigma \mathbf{E} \\ &= \mathbf{i}_{r_c} \left( \frac{\partial \varepsilon E_{r_c}}{\partial t} + \sigma E_{r_c} \right) + \mathbf{i}_\varphi \left( \frac{\partial \varepsilon E_\varphi}{\partial t} + \sigma E_\varphi \right) + \mathbf{i}_z \left( \frac{\partial \varepsilon E_z}{\partial t} + \sigma E_z \right), \end{aligned} \quad (6)$$

the components of electromagnetic field in Equations (5) and (6) along the same vector could be extracted like:

$$\frac{\partial H_z}{r_c \partial \varphi} - \frac{\partial H_\varphi}{\partial z} = \frac{\partial \varepsilon E_{r_c}}{\partial t} + \sigma E_{r_c}, \quad (7)$$

$$\frac{\partial H_{r_c}}{\partial z} - \frac{\partial H_z}{\partial r_c} = \frac{\partial \varepsilon E_\varphi}{\partial t} + \sigma E_\varphi, \quad (8)$$

$$\frac{H_\varphi}{r_c} + \frac{\partial H_\varphi}{\partial r_c} - \frac{\partial H_{r_c}}{r_c \partial \varphi} = \frac{\partial \varepsilon E_z}{\partial t} + \sigma E_z, \quad (9)$$

suggest that the electromagnetic property of MDLs satisfy  $\frac{\partial}{\partial \varphi} = 0$  due to the circular symmetry characteristic, then:

$$-\frac{\partial H_\varphi}{\partial z} = \frac{\partial \varepsilon E_{r_c}}{\partial t} + \sigma E_{r_c}, \quad (10)$$

$$\frac{\partial H_{r_c}}{\partial z} - \frac{\partial H_z}{\partial r_c} = \frac{\partial \varepsilon E_\varphi}{\partial t} + \sigma E_\varphi, \quad (11)$$

$$\frac{H_\varphi}{r_c} + \frac{\partial H_\varphi}{\partial r_c} = \frac{\partial \varepsilon E_z}{\partial t} + \sigma E_z, \quad (12)$$

Notably, the Equations (10)–(12) are similar to the two-dimensional FDTD equations in Cartesian coordinates except the term  $\frac{H_\varphi}{r_c}$ , which indicates that using the cylindrical coordinate FDTD simulation of MDL could reduce the dimensionality of the spatial grid, and wouldn't affect the precision of results. Besides the Ampère's circuital law with Maxwell's addition, the Maxwell–Faraday equation in cylindrical coordinate also satisfy this conclusion.

### 2.3. Efficiency Depends on Phase Levels

Extensive research has been conducted on the efficiency of MDLs, taking into account factors such as numerical aperture and the quantification of phase levels [28]. One of the key benefits of MDLs over FZPs is their construction of rings with varying heights, which facilitates the creation of multiple phase levels, thereby ensuring higher efficiency [29,30]. In comparison, FZPs often feature a binary structure, which may result in lower diffraction efficiency due to its limited phase variation capabilities [31]. The optical performance of MDLs is further improved by incorporating a multitude of height levels or phase steps, allowing for more precise control over the wavefront of light rays and enhancing the overall efficiency [32].

Researchers are continually examining the efficiency variations in MDLs that result from different phase level quantifications between  $0 - 2\pi$  [33–35]. It has been widely shown that the incorporation of additional height levels in MDLs enables more exacting control over light wavefront, leading to enhanced focal points and the rectification of optical aberrations. Through the meticulous regulation of phase at successive levels, MDLs can achieve greater diffraction efficiency and reduce unwanted optical artifacts.

Nevertheless, there is often a need to balance the sophistication of phase level precision with the practicalities of manufacturing. The quest for higher optical performance through finer phase quantification may be constrained by the limitations and expenses of producing lenses with an increased number of distinct height levels, necessitating a trade-off between optical precision and fabrication feasibility.

Intriguingly, the selection of quantification levels can also be strategically optimized. A pioneering approach has been introduced that employs varying phase quantifications across different regions of MDLs [36]. This method has demonstrated that satisfactory performance can be maintained, even when the outer zones are quantified with only 4 phase levels, while the central region is characterized by a higher degree of phase precision. This innovative strategy provides fresh insights into the quantification approaches for MDLs.

#### 2.4. Inverse Design

Designing MDLs often requires the application of inverse design method with advanced computational approaches and optimization strategies to achieve complex optical functions that are not readily computable through conventional principles, such as achromatization and enhancing depth of focus in lenses. To facilitate the design process, an array of cutting-edge computer-aided design and simulation tools has been developed [37,38].

The inverse design method initiates with the desired end result and then retraces the steps to engineer the required device or system specifications. This is in contrast to traditional design methods that start from known principles and make gradual improvements. Inverse design is unique in that it sets the target outcome first and then seeks the most suitable configuration to realize that goal.

One of the key advantages of inverse design is its ability to reveal innovative design solutions that could be overlooked by more traditional methods. It frees designers from conventional constraints, enabling them to explore novel configurations that may boost performance, efficiency, or functionality.

Inverse design frequently employs computational tools including optimization algorithms [39], machine learning [40,41], and artificial intelligence. These technologies aid in exploring the vast design space to identify the most effective solution that meets the predefined goals. Through iterative design parameter adjustments, the optimal configuration can be ascertained, ensuring the lens performs as intended, as illustrated in Figure 3b.

#### 2.5. MDLs with Sub-Wavelength Structure

The performance distinctions between MDLs and metalenses have been a topic of investigation [42]. A few studies have indicated that metalenses used for image projection do not necessarily outperform MDLs in terms of optical efficiency [43].

When it comes to metalenses, a defining feature is their sub-wavelength detailing [44]. With the current progress in micro-nano fabrication technologies, an increasing number of MDL structures are being realized with sub-wavelength dimensions. Consequently, several scholars have categorized MDLs with sub-wavelength structures as a subset of metalenses [24,25,45]. This indicates that the future evolution of MDLs is likely to embrace flexible design methodologies akin to those used for metalenses.

MDLs vs metalenses: Although MDLs with sub-wavelength structures sometimes could be considered as metalenses, there are some differences between them.

- Design approach: MDLs can be designed through inverse design techniques using cylindrical FDTD simulations, which offer high efficiency and accuracy. Conversely, metalenses are typically crafted by calculating meta-structures with the application of periodic boundary conditions, a process that might introduce minor inaccuracies when aligning the meta-structures.
- Material: MDLs have the flexibility to be manufactured from various materials utilizing dielectric materials with a high refractive index. In contrast, metalenses may incorporate metals along with materials of high refractive index to facilitate the required phase changes.
- Fabrication: MDLs are generally less complex and less costly to fabricate than metalenses, especially for large apertures. In comparison, the fabrication of metalenses tends to be more complex and expensive, owing to the fine precision needed to create their nanostructures.
- Polarization sensitivity: MDLs typically exhibit polarization insensitivity, maintaining consistent performance irrespective of the polarization of the incident light. In contrast, metalenses can be engineered to respond variably to different polarization states, a feature that may be advantageous or disadvantageous depending on the specific application requirements.

### 2.6. Achromatic MDLs

The sub-wavelength features and multilevel phase quantification of MDLs enable their potential for aberration correction across specific frequency bands, which is especially beneficial for broadband imaging applications. Theoretically, researchers have shown that MDLs can achieve a high numerical aperture (0.9) along with a broad operating bandwidth (300 nm within the visible spectrum) [46]. Comparative theoretical analyses of broadband performance among various planar lenses also highlight the potential of achromatic MDLs [47].

One approach to tackling chromatic aberration involves increasing the height of the MDL, effectively extending the phase quantification from 0 to  $n \cdot 2\pi$ . By employing a numerical method that minimizes an objective function representing the deviation between the complex transmission functions of the designed MDL at multiple wavelengths and the complex transmission functions of lenses with a focal distance  $f$  tailored for each wavelength, achromatic MDLs can be engineered [48]. This process necessitates optimization algorithms to find a satisfactory achromatic MDL [13,49].

Furthermore, the inverse design technique can be applied in the design of achromatic MDLs, integrating optimization algorithms with electromagnetic simulations [19,50]. This underscores the significant value of an efficient electromagnetic simulation, such as cylindrical coordinate FDTD. A variety of optimization algorithms could be utilized in this context, including differential evolution (DE) [50], particle swarm optimization (PSO) [19], genetic algorithms (GA), and stochastic gradient descent (SGD), among others.

## 3. Fabrication

The manufacturing of MDLs is significantly influenced by the progress in micro-nano fabrication technologies. Concurrently, these fabrication techniques have a direct impact on the performance characteristics of MDLs [51–54]. The complex, multilevel structures of MDLs have posed challenges for micro-nano fabrication [55]. Nonetheless, with the evolution of micro-nano fabrication technologies into more advanced and adaptable forms, the successful production of MDLs has been repeatedly achieved using various state-of-the-art methods. These include reactive ion etching (RIE) [56–59], lithography [60,61], and 3D printing [62]. Additionally, efforts are being made to apply antireflective coatings to MDLs to enhance their efficiency [63]. In this section, some of the most commonly utilized fabrication techniques for creating MDLs would be explored.

### 3.1. Electron Beam Lithography

Electron beam lithography (EBL) is a nanotechnology technique renowned for its precision and resolution in fabricating micro-nano structures. It entails focusing a precise electron beam onto a surface coated with an electron-reactive material, known as a resist, to etch the desired patterns. After patterning, the resist is developed and etched, transferring the design to the underlying substrate. EBL stands out for its sub-10 nanometer resolution, making it crucial for MDLs intended for visible light or shorter wavelengths.

EBL is especially proficient in creating binary diffractive lenses, such as FZPs, which are prized for their precise focus control. For instance, EBL has been effectively used to produce lenses that can finely tune the light's focal point, as depicted in Figure 4a [64]. While EBL is highly effective for creating binary structures, it might not be the best choice for devices requiring multilevel configurations.

For multilevel structures using EBL, the lithography must be repeated several times, as outlined in [65]. The intricacy of such designs can pose challenges, and the associated costs can be variable and potentially very high, which may render it less practical for producing MDLs.

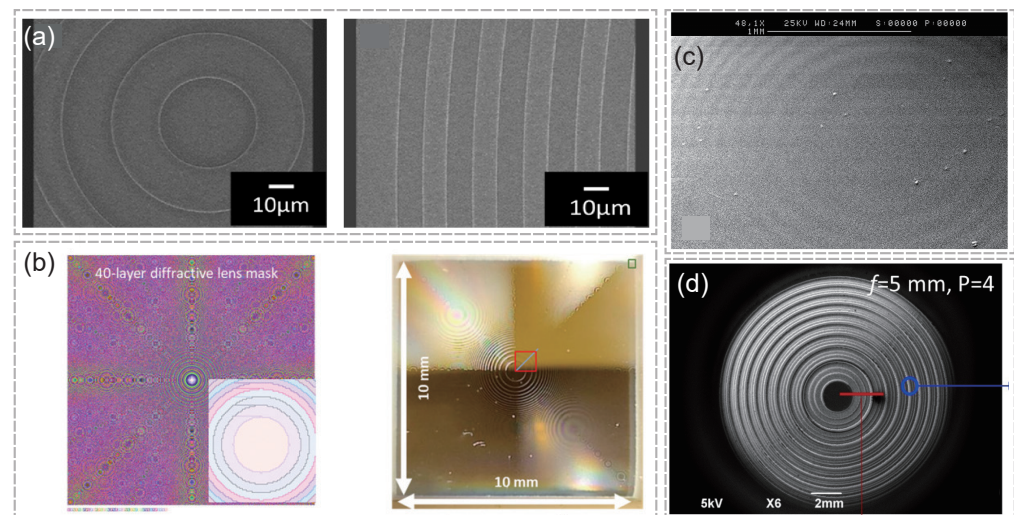


**Figure 4.** This figure showcases various examples of widely used fabrication technologies for MDLs. (a) A binary diffractive lens fabricated by EBL. Reprinted with permission from [64] © Optical Society of America. (b) A 40-layer diffractive lens produced on a photoresist layer atop a glass substrate by GSL, featuring a topographic range of approximately 10 μm and designed for operation at  $\lambda = 1550$  nm [66]. © 2022 Published by Elsevier B.V. under a Creative Commons CC-BY 4.0 License. (c) A diffractive lens manufactured using NIL, showing a sine-like radial relief of fabricated diffractive lens [67]. © The Authors. Published by SPIE under a Creative Commons Attribution 4.0 Unported License. (d) A 4-level MDL crafted through DLA with a laser system operating at a wavelength of 1064 nm, a pulse duration of 13 ps, a repetition rate of 1 MHz, and a peak energy of 60 μJ. Reprinted with permission from [68] © Optical Society of America.

### 3.2. Grayscale Lithography

To surmount the challenges associated with fabricating multilevel structures through EBL, grayscale lithography (GSL) has been developed, enabling the creation of substrate features with varying depths or heights [69,70]. Distinct from conventional lithography techniques that typically yield binary outcomes, GSL is capable of producing patterns with different levels of exposure or material removal, leading to three-dimensional structures with smooth gradients or steps in height.

GSL has proven particularly effective for crafting MDLs. For instance, a long-wavelength infrared (LWIR) MDL was manufactured using GSL on a silicon substrate for imaging purposes [71]. Additionally, a 40-layer diffractive lens, with a topographic range of approximately 10 μm and designed for operation at  $\lambda = 1550$  nm, has been realized on a photoresist layer over a glass wafer, as depicted in Figure 4b. This lens could be incorporated into a two-lens varifocal system [66].

### 3.3. Nanoimprint Lithography

Nanoimprint lithography (NIL) is a highly effective technique for creating multilevel structures. It is a cutting-edge nanofabrication method that allows for the high-resolution and precise patterning of nanostructures onto a range of substrates. During the NIL process, a template or mold with nanoscale features is applied onto a polymer resist, impressing the pattern onto the resist. The resist is subsequently cured and solidified, after which the template is removed, resulting in an exact replica of the pattern on the resist's surface.

NIL is recognized for its simplicity, high production efficiency, and scalability, which positions it as a potential technology for the economical production of nanoscale devices and structures.

In a recent development, researchers have successfully fabricated MDLs utilizing both GSL and NIL [72]. This approach has been shown to allow for the accurate creation of MDL microstructures with a error margin of 10%, highlighting excellent structure control capabilities and fabrication accuracy. Significantly, NIL has drastically reduced the fabrication time for MDLs, from 5 h to merely 10 min per unit.

### 3.4. Direct Laser Ablation

During micro-nano fabrication, various techniques are employed to etch patterns onto surfaces. Direct laser ablation (DLA) stands out as a particularly popular choice. DLA involves the use of a precision laser beam to inscribe or remove material from the surface of optical elements [73,74], creating patterns with resolutions that span from sub-micron to nanometer scales. This method facilitates the production of intricate, high-resolution micro-nano structures tailored to specific designs, making it ideal for the fabrication of multilevel architectures.

The lasers utilized in DLA are mode-locked and can emit pulses in the picosecond (ps) to femtosecond (fs) range. A series of terahertz MDLs with varying degrees of phase quantization, from binary to continuous profiles, have been documented [68]. These were created with a laser system operating at a wavelength of 1064 nm, a pulse duration of 13 ps, a repetition rate of 1 MHz, and a peak energy of 60  $\mu$ J. An example of a 4-level MDL among them is depicted in Figure 4d.

In addition to ps pulse lasers, there has been a growing trend in the use of fs pulse lasers for fabrication tasks. The feasibility of fabricating a 4-level terahertz MDL using fs laser ablation has been demonstrated [75]. Another instance of MDL fabrication using an fs laser was also presented, where the laser provided the shortest pulse duration of  $\tau = 156$  fs, maintained an average power of  $P = 5$  W at a repetition rate of 50 kHz, resulting in an energy per pulse of  $E = 100$   $\mu$ J [76].

### 3.5. Fused Deposition Modeling

Fused deposition modeling (FDM) is a form of additive manufacturing, commonly known as 3D printing, that employs a thermoplastic filament. This filament is heated to its melting temperature and then extruded layer by layer through a nozzle to construct a three-dimensional object. The printer head traverses a predetermined path, depositing the material continuously and allowing each layer to cool and solidify before the subsequent layer is deposited.

While FDM 3D printing may not match the fabrication precision of methods like lithography or DLA, it is well-suited for the production of MDLs intended for frequencies below the infrared spectrum, such as millimeter wave or terahertz wave. A range of phase binary diffractive lenses operating at 0.625 THz have been successfully created using a 3D printer [77]. Additionally, 3D printing has been utilized to fabricate MDLs for the 0.11–0.17 THz frequency band [19], a 21-level MDL produced via FDM 3D printing is showcased in Figure 5a. There are also instances of 3D printing being used for MDLs designed for lower frequencies; for example, a MDL for 10 GHz applications has been manufactured using FDM [78].

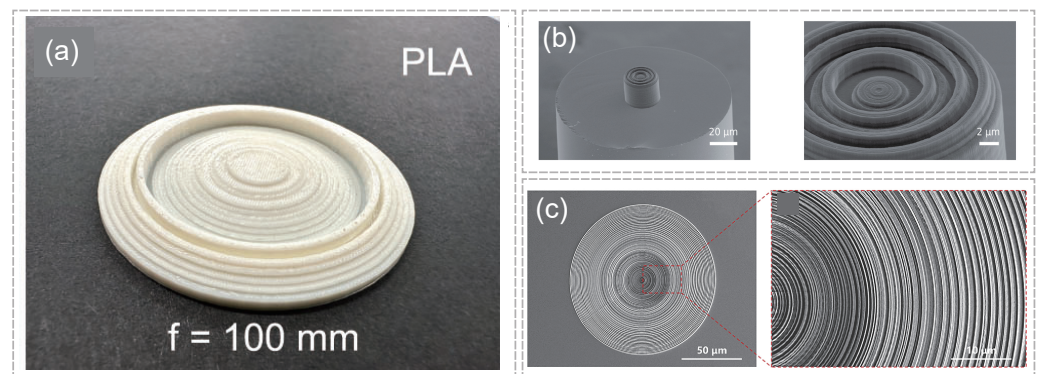


**Figure 5.** Several instances demonstrate the application of cutting-edge 3D printing technologies in the fabrication of MDLs. (a) A 21-level MDL created using FDM 3D printing technology working at 0.14 THz. Reprinted with permission from [19] © 2023 Chinese Optics Letters. (b) A MDL integrated onto the tip of an optical fiber, designed for operation at a wavelength of 780 nm, crafted through TPP 3D printing. Reprinted with permission from [79]. © 2021 American Chemical Society. (c) A single-layer, aberration-compensated supercritical lens operating at a wavelength of 633 nm, also produced using TPP 3D printing. Reprinted with permission from [80] © Optica Publishing Group.

### 3.6. Two-Photon Polymerization

Two-photon polymerization (TPP) is an advanced 3D printing technique that is gaining prominence in the fabrication of micro-optics and integrated optical components [81,82]. Offering greater precision than FDM 3D printing, TPP is well-suited for applications at infrared or visible wavelengths [83]. This method involves focusing a femtosecond laser into a photosensitive resin through a high NA microscope objective, which leads to a nonlinear absorption process where two photons are absorbed at once, initiating polymerization at the focus [84]. By steering the laser beam along a predefined path, intricate 3D structures can be crafted with high precision and fine details.

TPP has been extensively utilized in the production of MDLs. An example is an MDL fabricated on an optical fiber tip for operation at a wavelength of 780 nm, which achieved a focusing efficiency of 73% with a notably high NA of 0.85, as depicted in Figure 5b [79]. Additionally, a single-layer aberration-compensated supercritical lens for a working wavelength of 633 nm has been proposed, capable of sub-diffraction limited focusing within a 20° field of view, consisting of 300 concentric rings with a fixed lateral scale of 200 nm but varying thicknesses to achieve an eight-level phase modulation, as shown in Figure 5c [80]. A similar MDL designed for 633 nm operation [85] was also created using a femtosecond pulsed laser with a wavelength of 780 nm, a 100 fs pulse duration, and an 80 MHz repetition rate in the TPP 3D printing. Recently, an achromatic lens has been successfully demonstrated using TPP [86], featuring a multilayer structure.

In summary, an increasing number of researchers are exploring the use of 3D printing technology for the manufacture of MDLs, attracted by the convenience and efficiency of 3D printing, as well as the growing maturity of the technology, which now allows for the fabrication of high-precision structures.

## 4. Application

In contrast to conventional lenses, MDLs offer several advantages such as compactness, ease of integration, and the ability to handle the diffraction limit, rendering them particularly valuable for certain applications. Unlike metalenses, which are known for their polarization-sensitive properties and can exhibit varied effects depending on the polarization direction, MDLs are generally utilized in scenarios that require polarization insensitivity [39]. Additionally, MDLs tend to be more straightforward to manufacture with large apertures when compared to metalenses. In this section, several applications of MDLs would be explored.

#### 4.1. Integration

Leveraging their compactness factor, MDLs can be more readily incorporated into optical systems. They are especially advantageous in applications that demand lightweight optical components, making MDLs a suitable alternative to conventional bulky lenses. A case in point is the ultra-lightweight harmonic diffractive lens deployed in the 3U CubeSat nanosatellite launched in March 2021 for Earth remote sensing [87]. Furthermore, MDLs can be integrated with fiber tips [88], working together for light focusing, collimation, coupling to a light source, beam tailoring, and also for imaging and trapping applications.

#### 4.2. Imaging

Similar to metalenses, MDLs are capable of delivering resolutions that surpass the diffraction limit, which enables the visualization of intricate structures and details that conventional lenses might struggle to capture. Moreover, MDLs can be engineered for a variety of specialized imaging systems serving diverse objectives. They can notably extend the depth-of-focus across multiple wavelengths, also mitigating the limitations associated with larger aberrations and achieving achromatic focusing and imaging within a specific wavelength range [14].

Additionally, MDLs can be designed to possess multifocal capabilities, allowing them to focus different wavelengths at their respective desired focal lengths [65,89]. They are also adept at managing both high NA and broadband imaging in a single setup [90].

With the assistance of MDLs, innovative approaches and algorithms have been developed for lensless, full-color computational imaging. The innovation lies not only in the design and optimization techniques for MDLs but also in the novel definition of the point spread function (PSF) for RGB imaging with a broadband input light and the computational inverse imaging based on sparse color image modeling for simultaneous RGB channels [91,92]. The imaging process utilizing MDLs is depicted in Figure 6a. Furthermore, the successful design and end-to-end optimization for computational imaging with a hybrid optical setup consisting of a single refractive lens and a diffractive phase-encoded multi-phase mask have been demonstrated, taking into account the aperture size, lens focal length, and the distance between the MDL and sensor as variables for optimizing diffractive achromatic extended depth-of-field imaging [93].

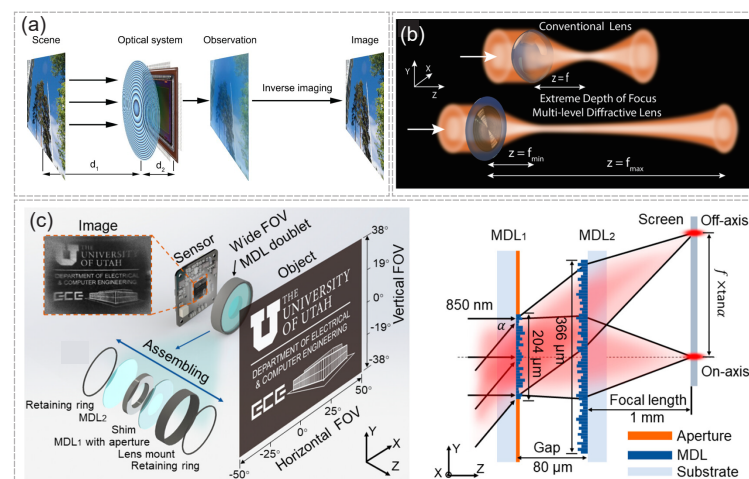


**Figure 6.** MDLs serve various imaging functionalities. (a) MDLs enable lensless, full-color computational imaging. Reprinted with permission from [91] © 2018 Informa UK Limited, trading as Taylor & Francis Group. (b) A MDL designed for extreme depth-of-focus imaging has been showcased, capable of focusing a beam across a range from 5 to 1200 mm. Reprinted with permission from [94] © Optical Society of America. (c) A multilevel diffractive doublet, consisting of two MDLs, has been demonstrated to achieve a  $100^\circ$  field of view (FOV) at  $\lambda = 850$  nm, offering high focusing efficiency and excellent resolution for imaging purposes. Reprinted with permission from [95]. © 2023 American Chemical Society.

A MDL designed for extreme depth-of-focus imaging, as shown in Figure 6b, has been developed to focus a beam across a range from 5 to 1200 mm. This demonstrates that new types of planar optics with large bandwidths and extensive DOF are feasible [94]. The use of a varifocal diffractive lens in multi-depth microscope imaging has also been showcased, highlighting the potential of flat shapeshifting optics as a foundation for next-generation optical systems [96].

A multilevel diffractive doublet, comprised of two MDLs, as illustrated in Figure 6c, has been demonstrated to achieve a  $100^\circ$  FOV at  $\lambda = 850$  nm, offering high focusing efficiency and excellent resolution for imaging [95]. Beyond the visible spectrum, the potential of MDLs for use in terahertz imaging has also been explored [97].

#### 4.3. 3D Display

Autostereoscopic 3D displays often encounter several critical challenges, including the need for a broad FOV, minimizing crosstalk and ghost image, achieving satisfactory light efficiency, resolving the vergence-accommodation conflict, and maintaining a compact design [15]. These issues can be mitigated through the use of planar optics, such as MDLs.

An example of this is a planar diffractive lens that manipulates the light field to create converged views across a significantly extended depth-of-field, providing high spatial resolution suitable for the human eye [98], as depicted in Figure 7a,b. In this instance, all the previously mentioned gaps were meticulously addressed, with a viewing distance that spans from 24 to 90 cm, an enhancement of the depth-of-field by a factor of  $1.8 \times 10^4$ -fold, crosstalk reduced to below 26% across a range of 66 cm, and light efficiency reaching 82%.

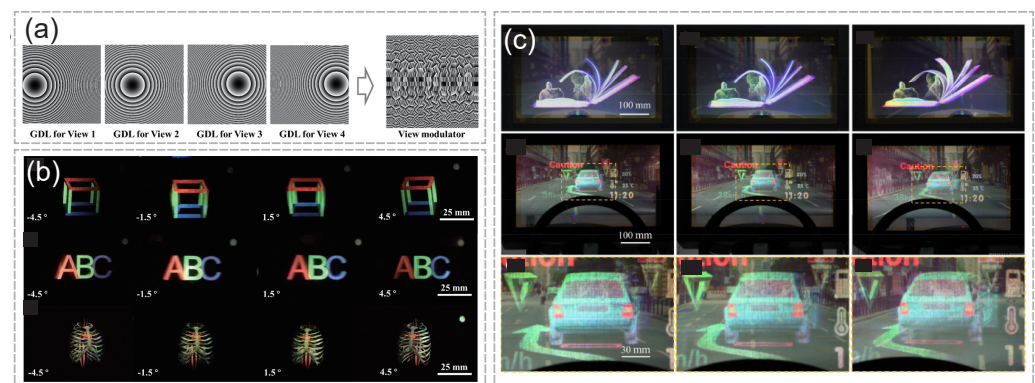


**Figure 7.** MDLs enhance the capabilities of 3D displays. (a) A diagram illustrating how a planar diffractive lens can modulate the light field to create converged views across an extended depth-of-field, offering high spatial resolution suitable for human vision. Reprinted with permission from [98] © Optica Publishing Group. (b) Visual representations of the vector light field 3D display as seen from various angles. Reprinted with permission from [98] © Optica Publishing Group. (c) The proposal of a large (20-inch) see-through combiner that utilizes 2,073,600 pixelated, intertwined MDLs for a full-color, glasses-free 3D display experience. Reprinted from [99], © 2024, with permission from Elsevier.

In recent developments, a sizeable (20-inch) see-through combiner has been conceptualized, utilizing 2,073,600 pixelated intertwined MDLs to enable a full-color, glasses-free 3D display [99], as depicted in Figure 7c. This setup has successfully achieved light efficiency rates of 30.57% for red, 30.68% for green, and 18.58% for blue light, respectively.

#### 4.4. Functional Devices in Optical Systems

In addition to their diverse applications, MDLs serve crucial roles in controlling light within numerous optical systems, such as those used in optical communication systems [19,100].

A single multi-focal MDL has been suggested to enhance the design of laser seekers, simultaneously improving both the linear measurement range and the measurement sensitivity of the seeker [101].

MDLs are also utilized for creating structured light. For instance, a demonstration of THz light being shaped into structured, self-accelerating, and nonlinearly propagating nonparaxial radiation has been showcased [76]. Additionally, there are examples of generating orbital angular momentum (OAM) light using a multilevel angular phase contour [102]. Moreover, a novel MDL, deviating from the typical circular symmetry, has been designed and experimentally tested for focusing high-power terahertz radiation into a square area [103].

## 5. Conclusions and Outlook

In this article, we present a comprehensive review of the evolution of MDLs, tracing their development from FZPs to MDLs and metalenses. We delve into the core principles underlying the design of MDLs, with an emphasis on inverse design methodologies and efficient electromagnetic simulation techniques. Subsequently, we examine the fabrication approaches that are commonly used in the production of MDLs. Furthermore, we highlight the potential of cutting-edge fabrication technologies, such as 3D printing, which show great promise for the manufacturing of MDLs, including FDM and TPP.

We also outline various applications where MDLs could be effectively utilized. The increasing significance of planar optics indicates that MDLs are poised to become a key element in future optical systems, serving vital functions in the realms of micro-nano optics, photonic computing, and virtual reality. Additionally, we believe that the design principles of metalenses could greatly enhance the design process for MDLs, revealing immense potential for the further advancement of MDL technology.

**Challenges:** The fabrication of MDLs with sub-wavelength features, similar to metalenses, often demands high-precision techniques, which can be difficult to accomplish, particularly for larger apertures or finer phase level quantification. Additionally, there is a need for the development of dielectric materials with higher refractive index suitable for MDLs. Furthermore, the inverse design methods used for MDLs face the challenge of requiring more efficiency and modernization, such as through the integration of neural networks or other advanced machine learning technologies.

**Future perspectives:** The advent of additive manufacturing technologies like FDM and TPP offers a higher degree of precision for the production of MDLs, enabling the achievement of more finely quantified phase levels. As inverse design strategies continue to evolve, it becomes possible to design MDLs with multifunctional capabilities aided by sub-wavelength structures, such as lenses with extended depth-of-focus and achromatic lenses, demonstrating a more versatile control over light manipulation.

**Author Contributions:** Conceptualization, S.C.; investigation, C.S. and W.Z.; resources, C.S. and W.Z.; writing—original draft preparation, C.S. writing—review and editing, S.C. and W.L.; visualization, C.S.; supervision, S.C. and W.L.; project administration, S.C. and W.L.; funding acquisition, S.C. and W.L. All authors have read and agreed to the published version of the manuscript.

**Funding:** This research was funded by National Natural Science Foundation of China (62375011, 52205603, 62005140), the Beijing Natural Science Foundation (L233019), the Ningbo Natural Science Foundation (2023J396).

**Data Availability Statement:** No new data were created or analyzed in this study. Data sharing is not applicable to this article.

**Conflicts of Interest:** The authors declare no conflict of interest.

## Abbreviations

The following abbreviations are used in this manuscript:

DE	Differential Evolution
DLA	Direct Laser Ablation
EBL	Electron Beam Lithography
FDM	Fused Deposition Modeling
FDTD	Finite-Difference Time-Domain
FOV	Field of View
FZP	Fresnel Zone Plate
GA	Genetic Algorithms
GSL	Grayscale Lithography
LWIR	Long-Wavelength Infrared
MDL	Multilevel Diffractive Lens
NA	Numerical Aperture
NIL	Nanoimprint Lithography
OAM	Orbital Angular Momentum
PSO	Particle Swarm Optimization
RIE	Reactive Ion Etching
SGD	Stochastic Gradient Descent
TPP	Two-Photon Polymerization

## References

- Saleh, B.E.; Teich, M.C. *Fundamentals of Photonics*; John Wiley & Sons: Hoboken, NJ, USA, 2019.
- Yu, N.; Capasso, F. Flat Optics with Designer Metasurfaces. *Nat. Mater.* **2014**, *13*, 139–150. [[CrossRef](#)] [[PubMed](#)]
- Siemion, A. Terahertz Diffractive Optics—Smart Control over Radiation. *J. Infrared Millim. Terahertz Waves* **2019**, *40*, 477–499. [[CrossRef](#)]
- Siemion, A. The Magic of Optics—An Overview of Recent Advanced Terahertz Diffractive Optical Elements. *Sensors* **2020**, *21*, 100. [[CrossRef](#)] [[PubMed](#)]
- Huang, K.; Qin, F.; Liu, H.; Ye, H.; Qiu, C.W.; Hong, M.; Luk'yanchuk, B.; Teng, J. Planar Diffractive Lenses: Fundamentals, Functionalities, and Applications. *Adv. Mater.* **2018**, *30*, 1704556. [[CrossRef](#)] [[PubMed](#)]
- Liu, D.; Wang, L.; Shi, H.; Gao, G.; Li, J.; Bian, J.; Fan, B.; Du, J. The Design of Multi-Wavelength Confocal Diffractive Optical Element Based on Set Operation. *Optik* **2023**, *277*, 170667. [[CrossRef](#)]
- Waldman, G.S. Variations on the Fresnel Zone Plate. *J. Opt. Soc. Am.* **1966**, *56*, 215–218. [[CrossRef](#)]
- Arsenault, H. Diffraction Theory of Fresnel Zone Plates. *J. Opt. Soc. Am.* **1968**, *58*, 1536–1536. [[CrossRef](#)]
- Simpson, M.; Michette, A. Imaging Properties of Modified Fresnel Zone Plates. *Opt. Acta Int. J. Opt.* **1984**, *31*, 403–413. [[CrossRef](#)]
- Swanson, G.J. *Binary Optics Technology: The Theory and Design of Multi-Level Diffractive Optical Elements*; Massachusetts Institute of Technology, Lincoln Laboratory: Lexington, MA, USA, 1989; Volume 854.
- Zhang, Z.; Guo, C.; Wang, R.; Hu, H.; Zhou, X.; Liu, T.; Xue, D.; Zhang, X.; Zhang, F.; Zhang, X. Hybrid-Level Fresnel Zone Plate for Diffraction Efficiency Enhancement. *Opt. Express* **2017**, *25*, 33676–33687. [[CrossRef](#)]
- Hayward, T.M.; Qadri, S.N.; Brimhall, N.; Santiago, F.; Christophersen, M.; Dunay, C.; Espinola, R.L.; Martin, H.; Menon, R. Multilevel Diffractive Lens in the MWIR with Extended Depth-of-Focus and Wide Field-of-View. *Opt. Express* **2023**, *31*, 15384–15391. [[CrossRef](#)]
- Yang, G.; Zhang, F.; Pu, M.; Li, X.; Ma, X.; Guo, Y.; Luo, X. Dual-Wavelength Multilevel Diffractive Lenses for near-Infrared Imaging. *J. Phys. D Appl. Phys.* **2021**, *54*, 175109. [[CrossRef](#)]
- Menon, R.; Brimhall, N. Perspectives on Imaging with Diffractive Flat Optics. *ACS Photonics* **2023**, *10*, 1046–1052. [[CrossRef](#)]
- Hua, J.; Qiao, W.; Chen, L. Recent Advances in Planar Optics-Based Glasses-Free 3D Displays. *Front. Nanotechnol.* **2022**, *4*, 829011. [[CrossRef](#)]
- Di Fabrizio, E.; Romanato, F.; Gentili, M.; Cabrini, S.; Kaulich, B.; Susini, J.; Barrett, R. High-Efficiency Multilevel Zone Plates for keV X-rays. *Nature* **1999**, *401*, 895–898. [[CrossRef](#)]
- Banerji, S.; Sensale-Rodriguez, B. Inverse Designed Achromatic Flat Lens Operating in the Ultraviolet. *OSA Contin.* **2020**, *3*, 1917–1929. [[CrossRef](#)]
- Swanson, G.J.; Veldkamp, W.B. Diffractive Optical Elements for Use in Infrared Systems. *Opt. Eng.* **1989**, *28*, 605–608. [[CrossRef](#)]
- Shi, C.; Wang, Y.; Liu, Q.; Chen, S.; Zhao, W.; Wu, X.; Cheng, J.; Chang, S. Inverse Design on Terahertz Multilevel Diffractive Lens Based on 3D Printing. *Chin. Opt. Lett.* **2023**, *22*, 110006. [[CrossRef](#)]
- Khorasaninejad, M.; Chen, W.T.; Devlin, R.C.; Oh, J.; Zhu, A.Y.; Capasso, F. Metalenses at Visible Wavelengths: Diffraction-limited Focusing and Subwavelength Resolution Imaging. *Science* **2016**, *352*, 1190–1194. [[CrossRef](#)]
- Chen, M.K.; Wu, Y.; Feng, L.; Fan, Q.; Lu, M.; Xu, T.; Tsai, D.P. Principles, Functions, and Applications of Optical Meta-Lens. *Adv. Opt. Mater.* **2021**, *9*, 2001414. [[CrossRef](#)]

22. Pan, M.; Fu, Y.; Zheng, M.; Chen, H.; Zang, Y.; Duan, H.; Li, Q.; Qiu, M.; Hu, Y. Dielectric Metalens for Miniaturized Imaging Systems: Progress and Challenges. *Light Sci. Appl.* **2022**, *11*, 195. [[CrossRef](#)]
23. Xu, Y.; Gu, J.; Gao, Y.; Yang, Q.; Liu, W.; Yao, Z.; Xu, Q.; Han, J.; Zhang, W. Broadband Achromatic Terahertz Metalens Constituted by Si-SiO<sub>2</sub>-Si Hybrid Meta-Atoms. *Adv. Funct. Mater.* **2023**, *33*, 2302821. [[CrossRef](#)]
24. Engelberg, J.; Levy, U. The Advantages of Metalenses over Diffractive Lenses. *Nat. Commun.* **2020**, *11*, 1991. [[CrossRef](#)] [[PubMed](#)]
25. Menon, R.; Sensale-Rodriguez, B. Inconsistencies of Metalens Performance and Comparison with Conventional Diffractive Optics. *Nat. Photon.* **2023**, *17*, 923–924. [[CrossRef](#)]
26. Shi, S.; Tao, X.; Yang, L.; Prather, D.W. Analysis of Diffractive Optical Elements Using a Nonuniform Finite-Difference Time-Domain Method. *Opt. Eng.* **2001**, *40*, 503–510. [[CrossRef](#)]
27. Prather, D.W.; Shi, S. Formulation and Application of the Finite-Difference Time-Domain Method for the Analysis of Axially Symmetric Diffractive Optical Elements. *J. Opt. Soc. Am. A* **1999**, *16*, 1131–1142. [[CrossRef](#)]
28. Levy, U.; Mendlovic, D.; Marom, E. Efficiency Analysis of Diffractive Lenses. *J. Opt. Soc. Am. A* **2001**, *18*, 86–93. [[CrossRef](#)]
29. Glytsis, E.N.; Harrigan, M.E.; Hirayama, K.; Gaylord, T.K. Collimating Cylindrical Diffractive Lenses: Rigorous Electromagnetic Analysis and Scalar Approximation. *Appl. Opt.* **1998**, *37*, 34–43. [[CrossRef](#)]
30. Prather, D.W.; Pustai, D.; Shi, S. Performance of Multilevel Diffractive Lenses as a Function of F-Number. *Appl. Opt.* **2001**, *40*, 207–210. [[CrossRef](#)]
31. Yamada, K.; Watanabe, W.; Li, Y.; Itoh, K.; Nishii, J. Multilevel Phase-Type Diffractive Lenses in Silica Glass Induced by Filamentation of Femtosecond Laser Pulses. *Opt. Lett.* **2004**, *29*, 1846–1848. [[CrossRef](#)]
32. Dou, W.B.; Wan, C. An Analysis of Diffractive Lenses at Millimeter Wavelengths. *Microw. Opt. Technol. Lett.* **2001**, *31*, 396–401. [[CrossRef](#)]
33. Cao, Q.; Jahns, J. Apodized Multilevel Diffractive Lenses That Produce Desired Diffraction-Limited Focal Spots. *J. Opt. Soc. Am. A* **2006**, *23*, 179–186. [[CrossRef](#)] [[PubMed](#)]
34. Rueda, E.; Muñetón, D.; Gómez, J.A.; Lencina, A. High-Quality Optical Vortex-Beam Generation by Using a Multilevel Vortex-Producing Lens. *Opt. Lett.* **2013**, *38*, 3941–3944. [[CrossRef](#)]
35. Mohapi, L.; Geiger, L.M.; Korvink, J.G.; Dudley, A.; Forbes, A. Simulating Multilevel Diffractive Optical Elements on a Spatial Light Modulator. *Appl. Opt.* **2022**, *61*, 7625–7631. [[CrossRef](#)] [[PubMed](#)]
36. Ayyagari, S.R.; Indrišiūnas, S.; Kašalynas, I. Hybrid Multi-Phase Fresnel Lenses on Silicon Wafers for Terahertz Frequencies. *IEEE Trans. Terahertz Sci. Technol.* **2023**, *13*, 231–236. [[CrossRef](#)]
37. Banerji, S.; Sensale-Rodriguez, B. A Computational Design Framework for Efficient, Fabrication Error-Tolerant, Planar THz Diffractive Optical Elements. *Sci. Rep.* **2019**, *9*, 5801. [[CrossRef](#)]
38. Banerji, S.; Meem, M.; Majumder, A.; Garcia, J.C.; Hon, P.; Pies, C.; Oberbiermann, T.; Menon, R.; Rodriguez, B.S. Inverse Designed Flat Optics with Multilevel Diffractive Lenses. In Proceedings of the Current Developments in Lens Design and Optical Engineering XXI, SPIE, Online Conference, 24 August–4 September 2020; Volume 11482, pp. 95–101. [[CrossRef](#)]
39. Yildirim, B.K.; Bor, E.; Kurt, H.; Turdnev, M. Zones Optimized Multilevel Diffractive Lens for Polarization-Insensitive Light Focusing. *J. Phys. D Appl. Phys.* **2020**, *53*, 495109. [[CrossRef](#)]
40. Jia, W.; Lin, D.; Menon, R.; Sensale-Rodriguez, B. Machine Learning Enables the Design of a Bidirectional Focusing Diffractive Lens. *Opt. Lett.* **2023**, *48*, 2425–2428. [[CrossRef](#)] [[PubMed](#)]
41. Jia, W.; Menon, R.; Sensale-Rodriguez, B. Reconfigurable and Programmable Optical Devices with Phase Change Materials Sb<sub>2</sub>S<sub>3</sub> and Sb<sub>2</sub>Se<sub>3</sub>. In Proceedings of the Active Photonic Platforms 2022, SPIE, San Diego, CA, USA, 21–26 August 2022; Volume 12196, pp. 12–18. [[CrossRef](#)]
42. Yang, F.; An, S.; Shalaginov, M.Y.; Zhang, H.; Rivero-Baleine, C.; Hu, J.; Gu, T. Design of Broadband and Wide-Field-of-View Metalenses. *Opt. Lett.* **2021**, *46*, 5735–5738. [[CrossRef](#)]
43. Meem, M.; Majumder, A.; Menon, R. Multi-Plane, Multi-Band Image Projection via Broadband Diffractive Optics. *Appl. Opt.* **2020**, *59*, 38–44. [[CrossRef](#)]
44. Pfeiffer, C.; Grbic, A. Planar Lens Antennas of Subwavelength Thickness: Collimating Leaky-Waves With Metasurfaces. *IEEE Trans. Antennas Propag.* **2015**, *63*, 3248–3253. [[CrossRef](#)]
45. Banerji, S.; Meem, M.; Majumder, A.; Vasquez, F.G.; Sensale-Rodriguez, B.; Menon, R. Imaging with Flat Optics: Metalenses or Diffractive Lenses? *Optica* **2019**, *6*, 805–810. [[CrossRef](#)]
46. Mohammad, N.; Meem, M.; Shen, B.; Wang, P.; Menon, R. Broadband Imaging with One Planar Diffractive Lens. *Sci. Rep.* **2018**, *8*, 2799. [[CrossRef](#)] [[PubMed](#)]
47. Engelberg, J.; Levy, U. Generalized Metric for Broadband Flat Lens Performance Comparison. *Nanophotonics* **2022**, *11*, 3559–3574. [[CrossRef](#)]
48. Doskolovich, L.L.; Skidanov, R.V.; Bezus, E.A.; Ganchevskaya, S.V.; Bykov, D.A.; Kazanskiy, N.L. Design of Diffractive Lenses Operating at Several Wavelengths. *Opt. Express* **2020**, *28*, 11705–11720. [[CrossRef](#)]
49. Wang, P.; Mohammad, N.; Menon, R. Chromatic-Aberration-Corrected Diffractive Lenses for Ultra-Broadband Focusing. *Sci. Rep.* **2016**, *6*, 21545. [[CrossRef](#)]
50. Yildirim, B.K.; Kurt, H.; Turdnev, M. Ultra-Compact, High-Numerical-Aperture Achromatic Multilevel Diffractive Lens via Metaheuristic Approach. *Photonics Res.* **2021**, *9*, 2095–2103. [[CrossRef](#)]

51. Ferstl, M.; Kuhlow, B.; Pawlowski, E. Effect of Fabrication Errors on Multilevel Fresnel Zone Lenses. *Opt. Eng.* **1994**, *33*, 1229–1235. [[CrossRef](#)]
52. Glytsis, E.N.; Harrigan, M.E.; Gaylord, T.K.; Hirayama, K. Effects of Fabrication Errors on the Performance of Cylindrical Diffractive Lenses: Rigorous Boundary-Element Method and Scalar Approximation. *Appl. Opt.* **1998**, *37*, 6591–6602. [[CrossRef](#)]
53. Britten, J.A.; Dixit, S.N.; DeBruyckere, M.; Steadfast, D.; Hackett, J.; Farmer, B.; Poe, G.; Patrick, B.; Atcheson, P.D.; Domber, J.L.; et al. Large-Aperture Fast Multilevel Fresnel Zone Lenses in Glass and Ultrathin Polymer Films for Visible and near-Infrared Imaging Applications. *Appl. Opt.* **2014**, *53*, 2312–2316. [[CrossRef](#)]
54. Banerji, S.; Cooke, J.; Sensale-Rodriguez, B. Role of Fabrication Errors and Refractive Index on Multilevel Diffractive Lens Performance. *Sci. Rep.* **2020**, *10*, 14608. [[CrossRef](#)]
55. Pitchumani, M.; Hockel, H.; Mohammed, W.; Johnson, E.G. Additive Lithography for Fabrication of Diffractive Optics. *Appl. Opt.* **2002**, *41*, 6176–6181. [[CrossRef](#)] [[PubMed](#)]
56. Pawlowski, E.; Engel, H. Multilevel Diffractive Optical Elements Fabricated with a Single Amplitude-Phase Mask. *Pure Appl. Opt. J. Eur. Opt. Soc. Part A* **1997**, *6*, 655. [[CrossRef](#)]
57. Walsby, E.D.; Wang, S.; Xu, J.; Yuan, T.; Blaikie, R.; Durbin, S.M.; Zhang, X.C.; Cumming, D.R.S. Multilevel Silicon Diffractive Optics for Terahertz Waves. *J. Vac. Sci. Technol. B Microelectron. Nanometer Struct. Process. Meas. Phenom.* **2002**, *20*, 2780–2783. [[CrossRef](#)]
58. Agafonov, A.N.; Volodkin, B.O.; Kaveev, A.K.; Knyazev, B.A.; Kropotov, G.I.; Pavel'ev, V.S.; Soifer, V.A.; Tukmakov, K.N.; Tsygankova, E.V.; Choporova, Y. Silicon Diffractive Optical Elements for High-Power Monochromatic Terahertz Radiation. *Optoelectron. Instrum. Data Proc.* **2013**, *49*, 189–195. [[CrossRef](#)]
59. Amata, H.; Fu, Q.; Heidrich, W. Additive Fabrication of SiO<sub>2</sub>-Based Micro-Optics with Lag-Free Depth and Reduced Roughness. *Opt. Express* **2023**, *31*, 41533–41545. [[CrossRef](#)]
60. Woo, D.K.; Hane, K.; Lee, C.B.; Lee, S.K. Fabrication of a Multi-Level Lens Using Independent-Exposure Lithography and FAB Plasma Etching. In Proceedings of the 2007 IEEE/LEOS International Conference on Optical MEMS and Nanophotonics, Hualien, Taiwan, 12–16 August 2007; pp. 151–152. [[CrossRef](#)]
61. Li, W.; He, P.; Yuan, W.; Yu, Y. Efficiency-Enhanced and Sidelobe-Suppressed Super-Oscillatory Lenses for Sub-Diffraction-Limit Fluorescence Imaging with Ultralong Working Distance. *Nanoscale* **2020**, *12*, 7063–7071. [[CrossRef](#)]
62. Jeong, K.H.; Ghalichechian, N. 3D-printed 4-Zone Ka-band Fresnel Lens: Design, Fabrication, and Measurement. *IET Microw. Antennas Propag.* **2020**, *14*, 28–35. [[CrossRef](#)]
63. Fluder, G.; Kowalik, A.; Rojek, A.; Sobczyk, A.; Choromański, Z.; Krężel, J.; Józwick, M. Analysis of the Influence of Antireflective Coatings on the Diffraction Efficiency of Diffractive Optical Elements. *Opt. Express* **2021**, *29*, 13025–13032. [[CrossRef](#)] [[PubMed](#)]
64. Motogaito, A.; Iguchi, Y.; Kato, S.; Hiramatsu, K. Fabrication and Characterization of a Binary Diffractive Lens for Controlling Focal Distribution. *Appl. Opt.* **2020**, *59*, 742–747. [[CrossRef](#)]
65. Britton, W.; Chen, Y.; Sgrignuoli, F.; Negro, L. Compact Dual-Band Multi-Focal Diffractive Lenses. *Laser Photon. Rev.* **2021**, *15*, 2000207. [[CrossRef](#)]
66. Aguiam, D.E.; Santos, J.D.; Silva, C.; Gentile, F.; Ferreira, C.; Garcia, I.S.; Cunha, J.; Gaspar, J. Fabrication and Optical Characterization of Large Aperture Diffractive Lenses Using Greyscale Lithography. *Micro. Nano. Eng.* **2022**, *14*, 100111. [[CrossRef](#)]
67. Osipov, V.P.; Doskolovich, L.L.; Bezus, E.A.; Drew, T.E.; Zhou, K.; Sawalha, K.; Swadener, G.; Wolffsohn, J.S.W. Application of Nanoimprinting Technique for Fabrication of Trifocal Diffractive Lens with Sine-like Radial Profile. *J. Biomed. Opt.* **2015**, *20*, 025008. [[CrossRef](#)] [[PubMed](#)]
68. Minkevičius, L.; Indrišiūnas, S.; Šniaukas, R.; Voisiat, B.; Janonis, V.; Tamošiūnas, V.; Kašalynas, I.; Račiukaitis, G.; Valušis, G. Terahertz Multilevel Phase Fresnel Lenses Fabricated by Laser Patterning of Silicon. *Opt. Lett.* **2017**, *42*, 1875–1878. [[CrossRef](#)] [[PubMed](#)]
69. Däschner, W.; Long, P.; Stein, R.; Wu, C.; Lee, S.H. Cost-Effective Mass Fabrication of Multilevel Diffractive Optical Elements by Use of a Single Optical Exposure with a Gray-Scale Mask on High-Energy Beam-Sensitive Glass. *Appl. Opt.* **1997**, *36*, 4675–4680. [[CrossRef](#)] [[PubMed](#)]
70. Wang, M.R.; Su, H. Multilevel Diffractive Microlens Fabrication by One-Step Laser-Assisted Chemical Etching upon High-Energy-Beam Sensitive Glass. *Opt. Lett.* **1998**, *23*, 876–878. [[CrossRef](#)]
71. Banerji, S.; Meem, M.; Majumder, A.; Guevara-Vasquez, F.; Menon, R.; Sensale-Rodriguez, B. Multi-Level Diffractive Lenses for Real-Time Long-Wave IR Imaging. In Proceedings of the 2019 44th International Conference on Infrared, Millimeter, and Terahertz Waves (IRMMW-THz), Paris, France, 1–6 September 2019; p. 1. [[CrossRef](#)]
72. Li, J.; Ge, S.; Liu, W. High-Efficiency and High-Precision Replication Manufacturing of Large-Aperture Multi-Level Diffractive Lenses. In Proceedings of the AOPC 2023: Optical Sensing, Imaging, and Display Technology and Applications; and Biomedical Optics, Beijing, China., 25–27 July 2023; Volume 12963, pp. 433–442. [[CrossRef](#)]
73. Wang, X.; Leger, J.R.; Rediker, R.H. Rapid Fabrication of Diffractive Optical Elements by Use of Image-Based Excimer Laser Ablation. *Appl. Opt.* **1997**, *36*, 4660–4665. [[CrossRef](#)]
74. Julian, M.N.; MacDonnell, D.G.; Gupta, M.C. High-Efficiency Flexible Multilevel Photon Sieves by Single-Step Laser-Based Fabrication and Optical Analysis. *Appl. Opt.* **2019**, *58*, 109–114. [[CrossRef](#)]

75. Komlenok, M.S.; Volodkin, B.O.; Knyazev, B.A.; Kononenko, V.V.; Kononenko, T.V.; Konov, V.I.; Pavelyev, V.S.; Soifer, V.A.; Tukmakov, K.N.; Choporova, Y.Y. Fabrication of a Multilevel THz Fresnel Lens by Femtosecond Laser Ablation. *Quantum Electron.* **2015**, *45*, 933. [[CrossRef](#)]
76. Ivaškevičiūtė-Povilauskienė, R.; Kizevičius, P.; Nacius, E.; Jokubauskis, D.; Ikamas, K.; Lissauskas, A.; Alexeeva, N.; Matulaitienė, I.; Jukna, V.; Orlov, S. Terahertz Structured Light: Nonparaxial Airy Imaging Using Silicon Diffractive Optics. *Light Sci. Appl.* **2022**, *11*, 326. [[CrossRef](#)]
77. Furlan, W.D.; Ferrando, V.; Monsoriu, J.A.; Zagrajek, P.; Czerwińska, E.; Szustakowski, M. 3D Printed Diffractive Terahertz Lenses. *Opt. Lett.* **2016**, *41*, 1748–1751. [[CrossRef](#)]
78. Yildirim, B.K.; Bor, E.; Kurt, H.; Turduduev, M. A Broadband Polarization-Insensitive Diffractive Lens Design for Subwavelength Focusing of Light. In Proceedings of the 2019 21st International Conference on Transparent Optical Networks (ICTON), Angers, France, 9–13 July 2019; pp. 1–4. [[CrossRef](#)]
79. Hadibrata, W.; Wei, H.; Krishnaswamy, S.; Aydin, K. Inverse Design and 3D Printing of a Metalens on an Optical Fiber Tip for Direct Laser Lithography. *Nano Lett.* **2021**, *21*, 2422–2428. [[CrossRef](#)] [[PubMed](#)]
80. Duan, H.; Wang, M.; Hu, X.; Li, Z.; Jiang, M.; Wang, S.; Cao, Y.; Li, X.; Qin, F. Aberration-Compensated Supercritical Lens for Sub-Diffractive Focusing within 20° Field of View. *Opt. Lett.* **2023**, *48*, 2523–2526. [[CrossRef](#)] [[PubMed](#)]
81. Wu, D.; Niu, L.G.; Chen, Q.D.; Wang, R.; Sun, H.B. High Efficiency Multilevel Phase-Type Fractal Zone Plates. *Opt. Lett.* **2008**, *33*, 2913–2915. [[CrossRef](#)] [[PubMed](#)]
82. Li, Y.; Yu, Y.; Guo, L.; Wu, S.; Chen, C.; Niu, L.; Li, A.; Yang, H. High Efficiency Multilevel Phase-Type Fresnel Zone Plates Produced by Two-Photon Polymerization of SU-8. *J. Opt.* **2010**, *12*, 035203. [[CrossRef](#)]
83. Wang, H.; Pan, C.F.; Li, C.; Menghrajani, K.S.; Schmidt, M.A.; Li, A.; Fan, F.; Zhou, Y.; Zhang, W.; Wang, H.; et al. Two-Photon Polymerization Lithography for Imaging Optics. *Int. J. Extreme Manuf.* **2024**, *6*, 042002. [[CrossRef](#)]
84. Vanmol, K.; Thienpont, H.; Ferranti, F.; Van Erps, J. Fabrication of Multilevel Metalenses Using Multiphoton Lithography: From Design to Evaluation. *Opt. Express* **2024**, *32*, 10190–10203. [[CrossRef](#)]
85. Hao, C.; Gao, S.; Ruan, Q.; Feng, Y.; Li, Y.; Yang, J.; Li, Z.; Qiu, C. Single-Layer Aberration-Compensated Flat Lens for Robust Wide-Angle Imaging. *Laser Photon. Rev.* **2020**, *14*, 2000017. [[CrossRef](#)]
86. Pan, C.F.; Wang, H.; Wang, H.; S, P.N.; Ruan, Q.; Wredh, S.; Ke, Y.; Chan, J.Y.E.; Zhang, W.; Qiu, C.W.; et al. 3D-printed Multilayer Structures for High-Numerical Aperture Achromatic Metalenses. *Sci. Adv.* **2023**, *9*, eadj9262. [[CrossRef](#)]
87. Ivliev, N.; Evdokimova, V.; Podlipnov, V.; Petrov, M.; Ganchevskaya, S.; Tkachenko, I.; Abrameshin, D.; Yuzifovich, Y.; Nikonorov, A.; Skidanov, R. First Earth-Imaging CubeSat with Harmonic Diffractive Lens. *Remote Sens.* **2022**, *14*, 2230. [[CrossRef](#)]
88. Piccirillo, F.; Giaquinto, M.; Ricciardi, A.; Cusano, A. Miniaturized Lenses Integrated on Optical Fibers: Towards a New Milestone along the Lab-on-Fiber Technology Roadmap. *Results Opt.* **2022**, *6*, 100203. [[CrossRef](#)]
89. Jia, W.; Lin, D.; Menon, R.; Sensale-Rodriguez, B. Multifocal Multilevel Diffractive Lens by Wavelength Multiplexing. *Appl. Opt.* **2023**, *62*, 6931–6938. [[CrossRef](#)] [[PubMed](#)]
90. Werdehausen, D.; Burger, S.; Staude, I.; Pertsch, T.; Decker, M. Flat Optics in High Numerical Aperture Broadband Imaging Systems. *J. Opt.* **2020**, *22*, 065607. [[CrossRef](#)]
91. Katkovnik, V.; Ponomarenko, M.; Egiazarian, K. Lensless Broadband Diffractive Imaging with Improved Depth of Focus: Wavefront Modulation by Multilevel Phase Masks. *J. Mod. Opt.* **2019**, *66*, 335–352. [[CrossRef](#)]
92. Rostami, S.R.; Katkovnik, V.; Egiazarian, K. Extended DoF and Achromatic Inverse Imaging for Lens and Lensless MPM Camera Based on Wiener Filtering of Defocused OTFs. *Opt. Eng.* **2021**, *60*, 051204–051204. [[CrossRef](#)]
93. MiriRostami, S.; Pinilla, S.; Shevkunov, I.; Katkovnik, V.; Egiazarian, K. Hybrid Diffractive Optics (DOE & Refractive Lens) for Broadband EDoF Imaging. *Electron. Imaging* **2023**, *35*, 1–14. [[CrossRef](#)]
94. Banerji, S.; Meem, M.; Majumder, A.; Sensale-Rodriguez, B.; Menon, R. Extreme-Depth-of-Focus Imaging with a Flat Lens. *Optica* **2020**, *7*, 214–217. [[CrossRef](#)]
95. Lin, D.; Hayward, T.M.; Jia, W.; Majumder, A.; Sensale-Rodriguez, B.; Menon, R. Inverse-Designed Multi-Level Diffractive Doublet for Wide Field-of-View Imaging. *ACS Photonics* **2023**, *10*, 2661–2669. [[CrossRef](#)]
96. Reda, F.; Salvatore, M.; Borbone, F.; Maddalena, P.; Ambrosio, A.; Oscurato, S.L. Varifocal Diffractive Lenses for Multi-Depth Microscope Imaging. *Opt. Express* **2022**, *30*, 12695–12711. [[CrossRef](#)]
97. Minkevičius, L.; Indrišiūnas, S.; Šniaukas, R.; Račiukaitis, G.; Janonis, V.; Tamošiūnas, V.; Kašalynas, I.; Valušis, G. Compact Diffractive Optics for THz Imaging. *Lith. J. Phys.* **2018**, *58*. [[CrossRef](#)]
98. Zhou, F.; Zhou, F.; Chen, Y.; Hua, J.; Qiao, W.; Chen, L. Vector Light Field Display Based on an Intertwined Flat Lens with Large Depth of Focus. *Optica* **2022**, *9*, 288–294. [[CrossRef](#)]
99. Shi, J.; Qiao, W.; Zhou, F.; Yang, M.; Chen, L. A See-through Combiner Based on Pixelated Intertwined Flat Lens for Full-Color Glasses-Free Augmented Reality. *Opt. Lasers Eng.* **2024**, *177*, 108147. [[CrossRef](#)]
100. Zarschizky, H.; Stemmer, A.; Mayerhofer, F.; Lefranc, G.; Gramann, W. Binary and Multilevel Diffractive Lenses with Submicrometer Feature Sizes. *Opt. Eng.* **1994**, *33*, 3527–3536. [[CrossRef](#)]
101. Ūnal, A. Laser Seeker Design with Multi-Focal Diffractive Lens. *Eng. Res. Express* **2023**, *5*, 045014. [[CrossRef](#)]

102. Vijayakumar, A.; Rosales-Guzmán, C.; Rai, M.R.; Rosen, J.; Minin, O.V.; Minin, I.V.; Forbes, A. Generation of Structured Light by Multilevel Orbital Angular Momentum Holograms. *Opt. Express* **2019**, *27*, 6459–6470. [[CrossRef](#)]
103. Komlenok, M.S.; Kononenko, T.V.; Konov, V.I.; Choporova, Y.Y.; Osintseva, N.D.; Knyazev, B.A.; Pavelyev, V.S.; Tukumakov, K.N.; Soifer, V.A. Silicon Diffractive Optical Element with Piecewise Continuous Profile to Focus High-Power Terahertz Radiation into a Square Area. *J. Opt. Soc. Am. B* **2021**, *38*, B9–B13. [[CrossRef](#)]

**Disclaimer/Publisher’s Note:** The statements, opinions and data contained in all publications are solely those of the individual author(s) and contributor(s) and not of MDPI and/or the editor(s). MDPI and/or the editor(s) disclaim responsibility for any injury to people or property resulting from any ideas, methods, instructions or products referred to in the content.